Received: 23 July 2021 | Revised: 27 December 2021 | Accepted: 4 January 2022

DOI: 10.1002/dep2.175

The Depositional Record Open Access
A journal of the International Association of Sedimentologists
WILEY

ORIGINAL ARTICLE

Earth's oldest tsunami deposit? Early Archaean high-energy sediments in the *ca* 3.48 Ga Dresser Formation (Pilbara, Western Australia)

Eric A. Runge[1,2] | **Jan-Peter Duda**[1,3] | **Martin J. Van Kranendonk**[4] | **Joachim Reitner**[2,3]

[1]Sedimentology and Organic Geochemistry, Center for Applied Geosciences, Eberhard-Karls-University Tübingen, Tübingen, Germany

[2]Geobiology, Geoscience Centre, Georg-August-Universität Göttingen, Göttingen, Germany

[3]"Origin of Life" Group, Göttingen Academy of Sciences and Humanities, Göttingen, Germany

[4]Australian Centre for Astrobiology, School of Biological, Earth and Environmental Sciences, University of New South Wales, Kensington, New South Wales, Australia

Correspondence
Joachim Reitner, Geobiology, Geoscience Centre, Georg-August-Universität Göttingen, Goldschmidtstraße 3, Göttingen, Germany.
Email: jreitne@gwdg.de

Funding information
Deutsche Forschungsgemeinschaft, Grant/Award Number: Du1450/3-1, Du1450/3-2, Du1450/7-1, Re665/42-2 and Th713/13-2; Australian Research Council, Grant/Award Number: CE1101017 and DP180103204

Abstract

Dynamic sedimentary processes are a key parameter for establishing the habitability of planetary surface environments on Earth and beyond and thus critical for reconstructing the early evolution of life on our planet. This paper presents a sedimentary section from the *ca* 3.48 Ga Dresser Formation (Pilbara Craton, Western Australia) that contains high-energy reworked sediments, possibly representing the oldest reported tsunami deposit on Earth to date. Field and petrographic evidence (e.g. up to 20 cm large imbricated clasts, hummocky bedding, Bouma-type graded sequences) indicate that the high-energy deposit represents a bi-directional succession of two debrite–turbidite couplets. This succession can best be explained by deposition related to passage and rebound of tsunami waves. Sedimentary processes were possibly influenced by highly dense silica-rich seawater. The tsunami was probably triggered by local fault-induced seismic activity since the Dresser Formation was deposited in a volcanic caldera basin that experienced syndepositional extensional growth faulting. However, alternative triggers (meteorite impact, volcanic eruption) or a combination thereof cannot be excluded. The results of this work indicate a subaquatic habitat that was subject to tsunami-induced high-energy disturbance. Potentially, this was a common situation on the early Archaean Earth, which experienced frequent impacts of extraterrestrial bodies. This study thus adds to the scarce record of early Archaean high-energy deposits and stresses the relevance of high-energy depositional events for the early evolution of life on Earth.

KEYWORDS

carbonates, depositional events, early life, habitability, high-energy deposits, seawater chemistry

1 | INTRODUCTION

Life has flourished in Earth's surface environments for at least 3.5 byr (Arndt & Nisbet, 2012; Lepot, 2020; Lowe, 1980) but the nature of these earliest habitats remains poorly constrained. Dynamic sedimentary processes are a key control on environmental conditions throughout geological time (Mata & Bottjer, 2012). In particular, high-energy events, such as tsunamis, can have a major impact on marine environments (Bahlburg & Spiske, 2012; Einsele et al., 1996). These tsunami events affect habitats via disturbance of surface sediments or redistribution of nutrients in the water column (Kanaya et al., 2015; Lowe et al., 2003; Noda et al., 2007). Supposed highly frequent impacts of extraterrestrial bodies in the early Archaean suggest that these tsunami-induced disturbances commonly affected the habitats of the earliest life (Lowe & Byerly, 2018). Therefore, reconstructing tsunami events is important for understanding the habitability of the earliest environments on Earth and, perhaps, on other planetary bodies.

Reported tsunami deposits from the Kaapvaal and Pilbara cratons date back to the early Archaean (Byerly, 2002; Glikson et al., 2004, 2016; Hassler et al., 2000; Hassler & Simonson, 2001). These ancient tsunami deposits are commonly interpreted to be related to impacts of extraterrestrial bodies because the high-energy sediments are associated with reworked impact ejecta material that contains impact spherules, shock metamorphosed mineral grains and/or cosmochemical fingerprints (e.g. siderophile element enrichments, chondritic isotope ratios). Although the Archaean Earth was supposedly affected by very abundant extraterrestrial impacts (Krull Davatzes et al., 2019), such direct geological evidence seems rare, which is perhaps partly due to later alteration and erosion (Simonson & Glass, 2004). Therefore, sedimentological features of high-energy deposits appear to be particularly important to track tsunami deposits in deep time. Tsunami deposits are commonly characterised by normally and/or inversely graded coarse-grained layers within fine-grained deep-water sediments, cross-stratification, erosive basal contacts, rip-up clasts, soft-sediment deformation and seaward flow structures indicating return flows (Costa & Andrade, 2020; Costa et al., 2012; Jaffe et al., 2012; Riou et al., 2018, 2020). Identifying these features in the Archaean depositional record is critical to reconstruct how tsunami events shaped Earth's earliest habitats.

Discussed herein is a high-energy deposit within the 3481 ± 3.6 Ma Dresser Formation (Warrawoona Group, Pilbara Craton, Western Australia), demonstrably one of the earliest, well-preserved habitats of life on Earth (Baumgartner et al., 2019; Djokic et al., 2017; Duda et al., 2018; Mißbach et al., 2021; Ueno et al., 2008; Van Kranendonk et al., 2008). By combining detailed field observations and petrographic analyses (including Raman spectra of minerals and μXRF geochemical imaging), a tsunami origin is inferred for the Dresser high-energy deposit, probably triggered by local growth faulting-induced seismic activity. The Dresser tsunami deposit slightly predates the previously earliest known geological evidence for tsunamis on Earth (i.e. 3.47 Ga impact ejecta beds: Byerly, 2002; Glikson et al., 2004) and thus extends the geological record of tsunami events and highlights the relevance of high-energy depositional events for Earth's earliest habitats.

2 | MATERIALS AND METHODS

The studied sedimentary section (21.155317°S; 119.436853°E) is located *ca* 500 m south-east of the former Dresser mine (Figure 1A). During fieldwork, the sampled section was observed, measured, documented and sampled for subsequent analyses. Petrographic thin sections (polished, *ca* 60 μm thick) were prepared of all samples and studied using a Zeiss SteREO Discovery.V8 stereomicroscope linked to an AxioCam MRc 5-megapixel camera.

Raman spectra were obtained using a Horiba Jobin YvonLabRam-HR 800 UV spectrometer with a focal length of 800 mm. The spectrometer was linked to an Olympus BX41 microscope. An argon ion laser (Melles Griot IMA 106020BOS, 488 nm) with a power of 50 mW was used for excitation of the sample. The laser beam was focussed with an Olympus MPane 100× objective with a numerical aperture of 0.9 and a confocal pinhole of 100 μm. It was then dispersed by a 600 l/mm grating on a CCD detector with 1024 × 256 pixels, yielding a spectral resolution of <2 cm^{-1} per pixel. Data were acquired over 5 s for a spectral range of 100–2000 cm^{-1}. The spectrometer was calibrated by using a silicon standard with a major peak at 520.4 cm^{-1}. All spectra were recorded and processed using the LabSpecTM database (version 5.19.17; Jobin-Yvon, Villeneuve d´ Asq, France).

Geochemical imaging was done using a Bruker M4 Tornado μXRF instrument equipped with a XFlash 430 Silicon Drift Detector. The X-ray tube was operating at 50 kV voltage and 400 μA amperage. The X-ray beam had a spot size of 25 μm. The chamber pressure was 20 mbar.

3 | RESULTS

The studied sedimentary succession is *ca* 5 m thick, outcrops over about 100 m along strike, and is interbedded with well-preserved pillow basalts of the Dresser Formation (Figure 1B). The studied succession consists mostly of brownish weathered, thinly bedded carbonate, but also contains

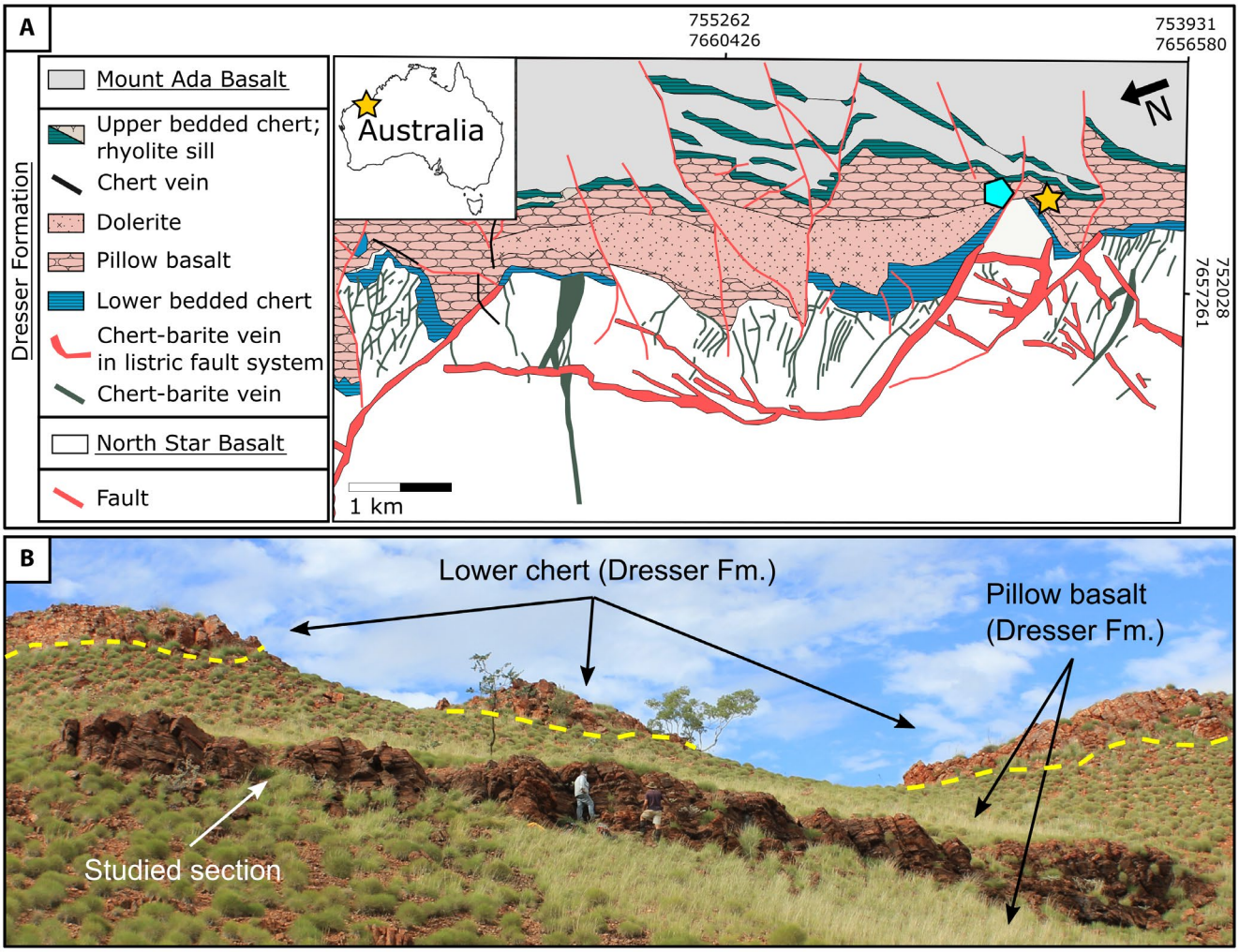

FIGURE 1 Spatial context of the studied section. (A) Location and geological map of the Dresser Formation near the studied section (yellow star) showing association with pillow basalt bedrock and listric growth faults. The locality of the Dresser mine (cyan pentagon) is provided for reference. Stratigraphic units in the legend are underlined. The map projection is Universal transverse Mercator (UTM) zone 50K (modified from (Van Kranendonk et al., 2019a); (B) studied section and its surroundings (people for scale)

some chert and jasper beds, as well as units of coarse conglomerate with massive carbonate (Figures 2 and 3). Based on its distinct lithologic characteristics, the studied succession can be divided into three units (Figure 2).

Unit 1 is *ca* 3.1 m thick and directly overlays well-developed pillow basalts of the Dresser Formation (Figures 1 and 2). This unit consists mostly of millimetre-scale bedded micritic carbonates with minor chert (Figures 2A and 4A,B), 1–6 cm thick chert beds, and a *ca* 0.5 m thick bed consisting of centimetre-scale interlayers of grey chert and jasper (Figure 2). The overlying, *ca* 0.5 m thick, Unit 2 is the most prominent feature of the section and shows evidence for reworking and redeposition of chert and carbonate sedimentary materials (Figures 2B, 3, 4 and 5). The uppermost Unit 3 is *ca* 1.4 m thick and dominated by black chert and jasper (Figure 2C).

Unit 2 can be subdivided into two subunits, each consisting of a chert clast-bearing layer at the base ('basal breccia') and a fine-grained chert-cemented carbonate layer at the top (Figures 3A,F, 4 and 5). The lower subunit is *ca* 30 cm thick and overlies grey chert of Unit 1 with a sharp planar contact (Figure 3A). The basal breccia of the lower subunit is generally *ca* 15 cm thick but locally much thinner, or completely absent. It is generally matrix-supported and in some places inversely graded (Figure 3B). Locally, the surface of the basal breccia of this subunit exhibits hummocky bedding (Figure 3C). Chert clasts in the basal breccia range between *ca* 1–20 cm, exhibit subangular to angular outlines, and consist of grey chert that is lithologically similar to the underlying chert beds (Figure 3A through D). Some clasts are imbricated at varying angles (representative strike and dip values, corrected for post-depositional tilting, at 310°/16°NE and 298°/24°NE) (Figure 3A,B), while others appear to be horizontally oriented (Figure 3C,D). The matrix of the basal breccia is poorly sorted and consists of up to 200 μm carbonate

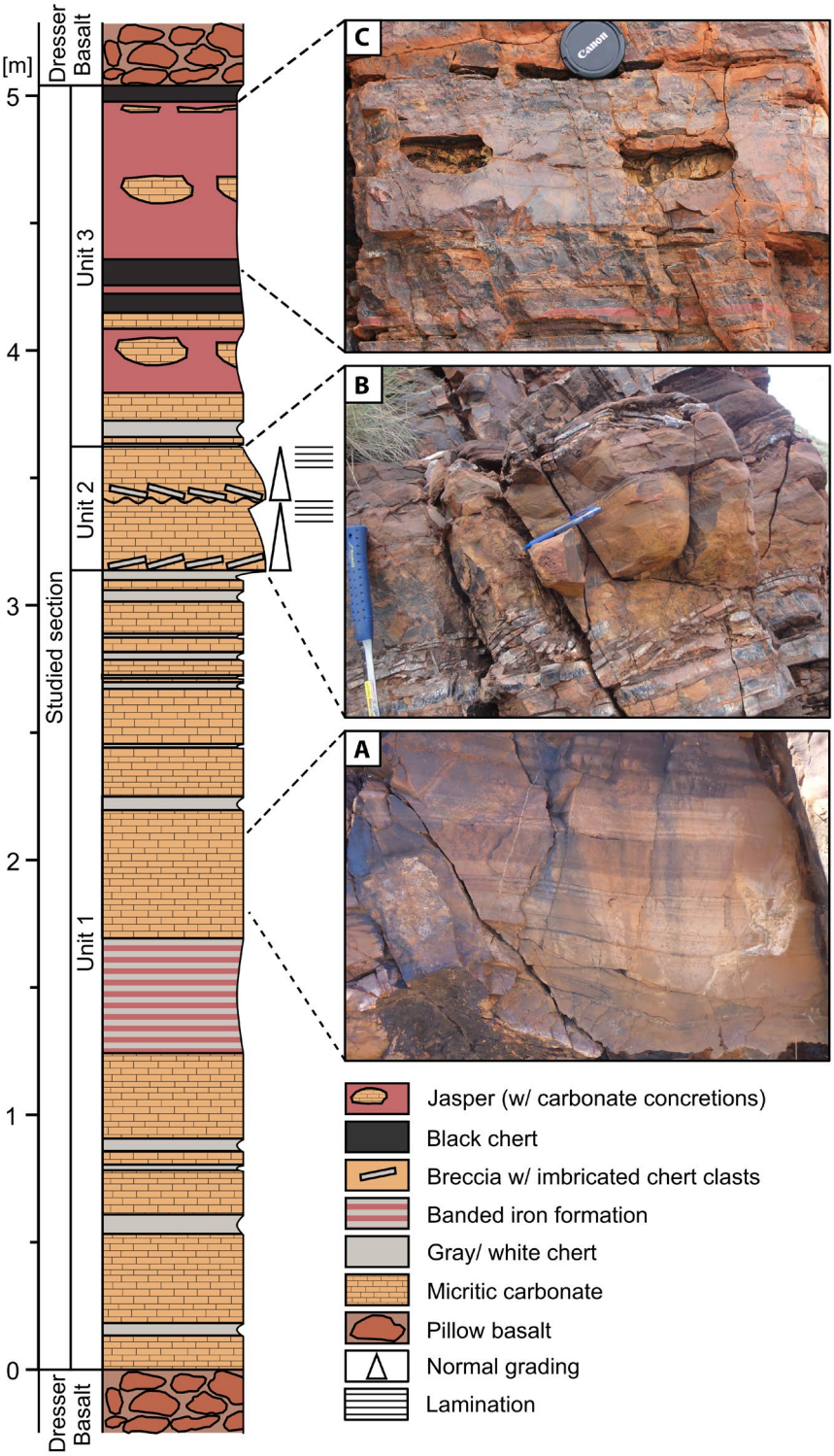

FIGURE 2 Lithological profile of the studied section. (A) Finely laminated micritic carbonates in Unit 1; (B) carbonate and chert sediments in Unit 2, showing evidence for sediment reworking and redeposition; (C) jasper and black chert in Unit 3

grains and up to millimetre-sized angular to subrounded chert grains (Figure 4C,E). The transition from the basal breccia to the overlying carbonate layer in the lower subunit is characterised by a marked decrease in grain size to below *ca* <20 μm. The thickness of the carbonate layer varies between *ca* 2 and 20 cm and is normally graded from a massive fabric at its base to one with a distinct lamination with local soft-sediment deformation structures at its top (Figure 3E). Some *ca* 3–5 cm isolated chert clasts lie within this carbonate layer (Figure 3B). Locally, the carbonates directly atop the basal breccia exhibit millimetre-scale sigmoidal crossbedding (Figure 4D).

The upper subunit of Unit 2 is only 20 cm thick (Figures 2 and 3A,F), with a basal breccia that is *ca* 10 cm thick and directly overlies the laminated carbonates of the lower subunit. The lower surface of the basal breccia is locally wavy (Figure

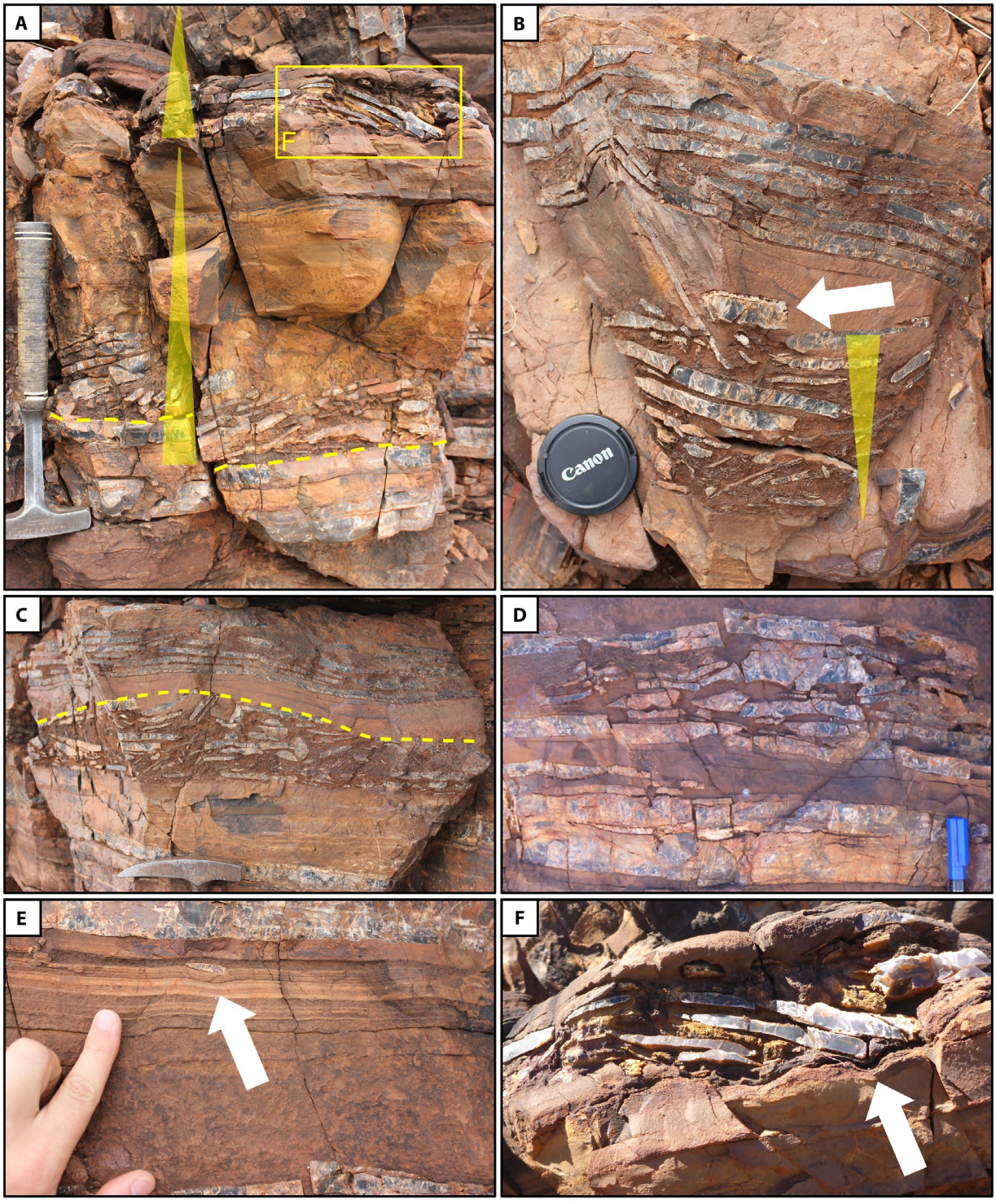

FIGURE 3 Sedimentology of Unit 2. (A) Overview of Unit 2 showing two subunits (yellow triangles), each with a basal breccia grading into massive fine-grained carbonates. Both subunits are interpreted as debrite–turbidite couplets. Note that the lower subunit directly overlies grey chert of Unit 1 (yellow dashed line) and that the clasts in both subunits are imbricated in opposite directions; (B) inverse grading in the basal breccia of the lower subunit (yellow triangle). Note that angular clasts float within fine-grained carbonates (white arrow); (C) basal breccia of the lower subunit showing hummocky bedding (yellow dashed line); (D) densely packed subangular to angular grey chert clasts in the basal breccia of the lower subunit; E: laminated carbonate deposits from the top of the lower subunit showing soft-sediment deformation (white arrow); (F) Close up of area indicated in (A), showing erosive lower surface of the basal breccia in the upper subunit (white arrow)

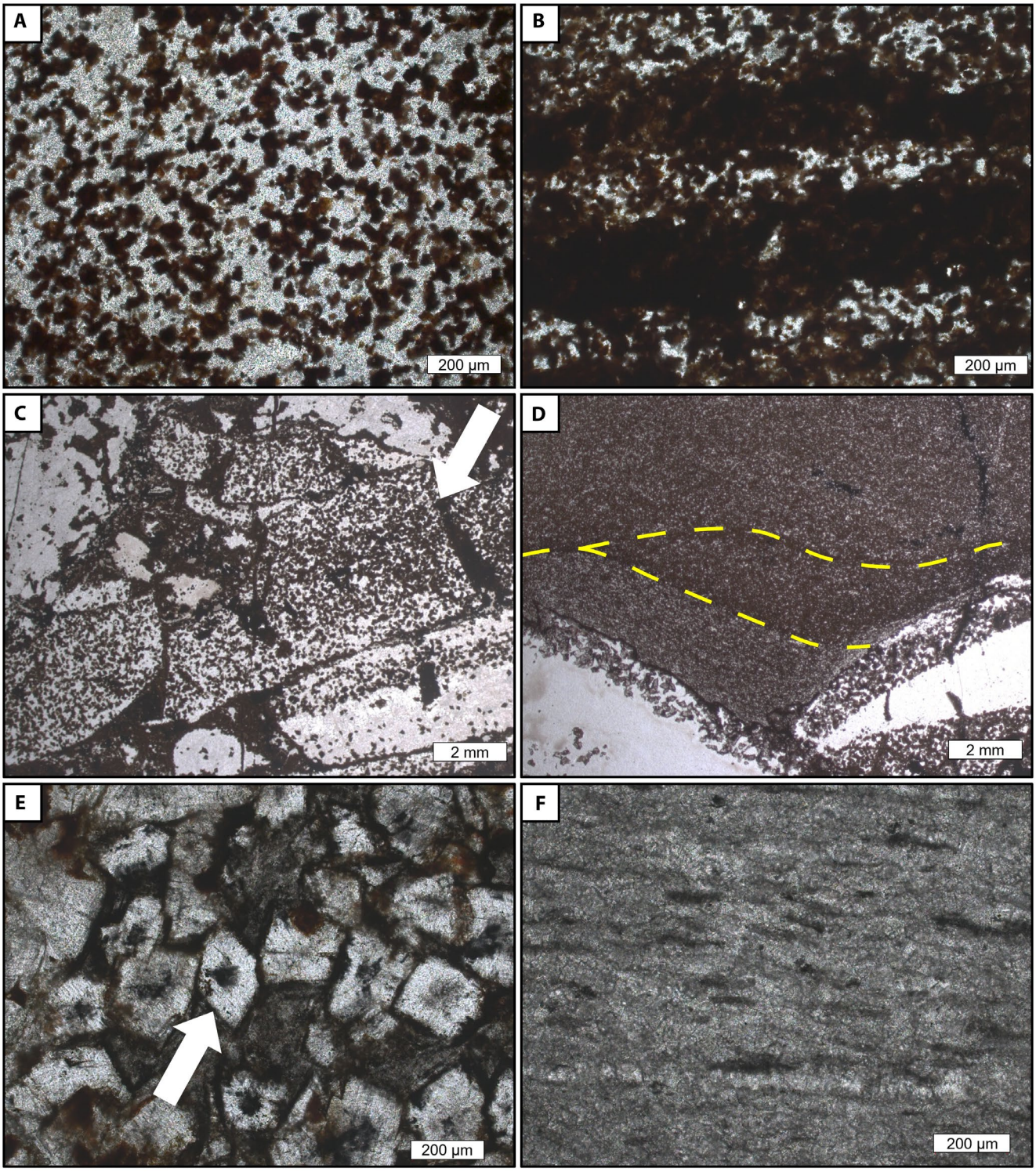

FIGURE 4 Transmitted light microscopy images of carbonates in Unit 1 (A, B) and the lower subunit in Unit 2 (C-F). A: micritic carbonates (brown) embedded within chert (grey); (B) mm-scale lamination in micritic carbonates (brown) embedded within chert; (C) angular chert clasts (white arrow) in the basal breccia of the lower subunit; (D) mm-scale sigmoidal crossbedding (yellow dashed lines) in fine-grained carbonates at the top of the basal breccia in the lower subunit, supporting sediment reworking and redeposition; (E) euhedral carbonate crystals (white arrow) in the matrix of the basal breccia of the lower subunit; (F) fine-grained laminated carbonates at the top of the lower subunit

3C) and exhibits erosional features (Figure 3A,F). Some of the chert clasts in the basal breccia of the upper subunit are imbricated, commonly in a reverse direction to those of the basal breccia of the lower subunit (representative strike and dip value: 076°/20°SSE: Figure 3A,F). The carbonate layer in the upper subunit is similar to that of the lower subunit.

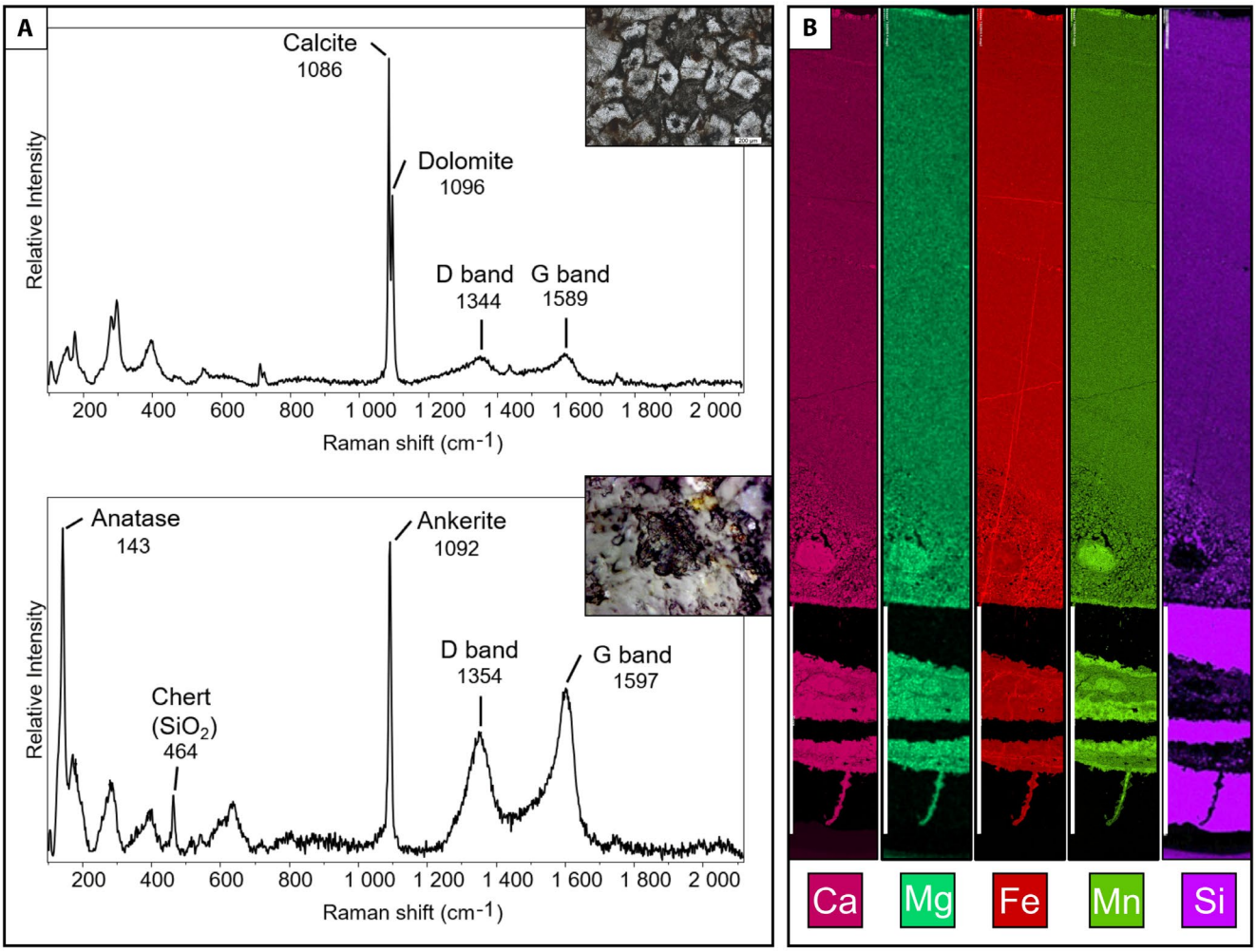

FIGURE 5 Raman spectroscopy spot analysis (A) and μXRF image scans of element distributions (B) in Unit 2. (A) representative Raman spectra from the carbonate layer in the lower subunit, supporting carbonate mineralogy and association with quartz (i.e. chert cementation), D and G-band represent sedimentary organic matter; (B) μXRF maps showing the distribution of Ca, Mg, Fe, Mn and Si (white scale bar is 2 cm). Co-enrichments of Ca, Mg, Fe and Mn correspond to carbonate minerals, while enrichments in Si reflect the presence of chert

4 | DISCUSSION

4.1 | Depositional Processes

The interbedding of the overall finely bedded sedimentary succession with well-developed pillow basalts (Figure 1B) indicates an interval of generally quiet-water sedimentation in between subaqueous lava eruption events. The fine-scale nature of the bedding in the majority of this succession and lack of sedimentary features indicative for wave agitation in the lower (Unit 1) and upper (Unit 3) parts of the succession (Figure 2A,C) indicate deposition in a low-energy subaqueous environment, probably below storm-wave base, in a submarine environment saturated in bicarbonate and in silica, depositing largely chemical sedimentary rocks (carbonate and chert). Coarse clast-bearing layers in Unit 2 (Figures 2B and 3), in contrast, show evidence for syndepositional erosion and reworking of lithified sediment, hence reflecting higher-energy depositional processes.

Notably, various characteristics of Unit 2, such as densely packed and locally imbricated clasts up to 20 cm in size, as well as chert pebbles 'floating' within fine-grained carbonates (Figure 3B through D), are consistent with deposition from a debris flow (Lowe, 1982). Furthermore, normal grading and the transition from massive to laminated fabric in the carbonates directly atop clast-bearing basal breccias of both subunits of Unit 2 are characteristic for Bouma and Lowe-type sequences and thus consistent with deposition from a high-density turbidity current (Bouma, 1962; Lowe, 1982) (Figures 3E and 6). Locally observed sigmoidal crossbedding in the fine-grained carbonates directly atop the breccia in the lower subunit supports a rapid progradational filling of the interspaces between

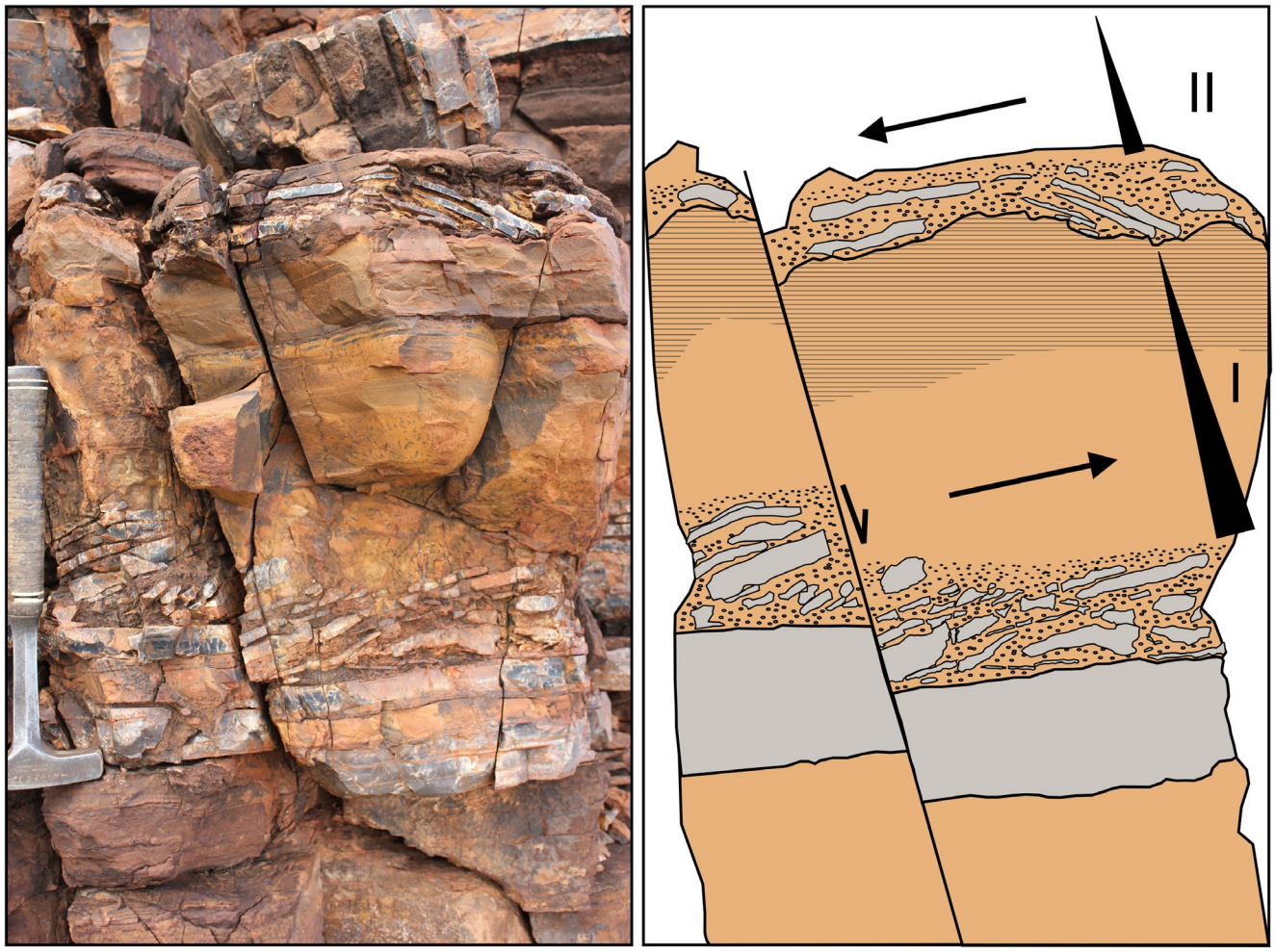

FIGURE 6 Photograph (left, hammer for scale) and sedimentological interpretation (right) of Unit 2 (I: lower subunit, II: upper subunit). Both subunits are interpreted as debrite–turbidite couplets that reflect the onflow and backwash phase of a tsunami event. Black triangles and arrows indicate normal grading and inferred transport directions respectively. Note the reduced thickness of the upper subunit as compared to the lower subunit. The graded carbonate deposits with a massive to laminated fabric resembles a Bouma or Lowe-type sequence. The succession exhibits evidence for post-lithification faulting, as indicated by the straight black line and half-arrow

the imbricated chert clasts (cf. Walker, 1978) (Figure 4D). Therefore, both subunits of Unit 2 are best interpreted as debrite–turbidite couplets.

The debrite layer of the upper subunit of Unit 2 directly overlies the turbidite-deposited carbonate part of the lower subunit across a contact that exhibits soft-sediment deformation structures and erosional features (Figure 3E,F). Hence, the turbidite layer of the lower subunit must have been unconsolidated during deposition of the debrite layer of the upper subunit. Moreover, the opposite direction of clast imbrication in both of the debrite layers (*ca* 300°/20°NE in the lower subunit vs. 076°/20°S in the upper subunit) indicates a switch in transport direction from south-west to north respectively (Figures 2B, 3A and 6). Such bi-directional sediment transport is commonly due to coupled onflow and backwash currents (Einsele et al., 1996) or flow rebound from a palaeotopographic high (Tada et al., 2002). This suggests that the upper subunit was deposited relatively soon after the lower subunit through a return flow ('backwash'), and that both subunits are thus related to a single depositional event. Moreover, hummocky bedding in the lower subunit indicates that these currents were associated with wave activity (Dumas & Arnott, 2006) (Figure 3C). In concert, these observations indicate that Unit 2 was deposited from bi-directional high-energy wave transport.

Bi-directional wave transport can result from inflow and backwash currents associated with storm or tsunami events (Einsele et al., 1996; Fujiwara & Kamataki, 2007). However, in settings below storm-wave base, storm deposits are usually unidirectional and form through backwash transport associated with storm surges (Benton & Gray, 1981; Morton et al., 2007). Moreover, backwash sediments in storm deposits are usually thicker and coarser than the respective inflow deposits (Morton et al., 2007). All these features are

inconsistent with the bi-directional flow structures of Unit 2, as well as with the reduced thickness and the local lack of chert clasts observed in the upper subunit, indicating a lower transport energy during the backwash phase of the event (Figures 2B and 6). Tsunami events, in contrast, can result in bi-directional transport below storm-wave base due to wave rebound on coastlines or topographic highs (Ikehara et al., 2014; Riou et al., 2018; Tada et al., 2002; Weiss & Bahlburg, 2006). Indeed, an energy loss upon wave rebound could plausibly explain the reduced thickness of the upper subunit of Unit 2. For these reasons, it is suggested that the subunits of Unit 2 reflect the inflow and subsequent backwash of a tsunami event.

The studied succession records a distinct sequence of depositional processes (Figure 7). Unit 1 formed from sedimentation of fine-grained carbonates and episodic silica under low-energy conditions (Figure 7A). Seismic disturbance initiated a tsunami wave which mobilised carbonate mud and chert clasts, triggering a high-density turbidity current (Figure 7B). From this current, the first debrite–turbidite couplet was deposited in a decelerating flow regime upon decreasing wave agitation and formed the lower subunit of Unit 2 (Figure 7C). The subsequent backwash initiated a second high-density turbidity current, which reworked previously deposited sediments and partly eroded the lower subunit of Unit 2 (Figure 7D). From this current, a second debrite–turbidite couplet was deposited and formed the upper subunit of Unit 2, which had a reduced thickness due to the loss of energy upon wave rebound (Figure 7D). Unit 3 documents a return to quiet-water sedimentation of fine-grained carbonates and silica (Figure 7E).

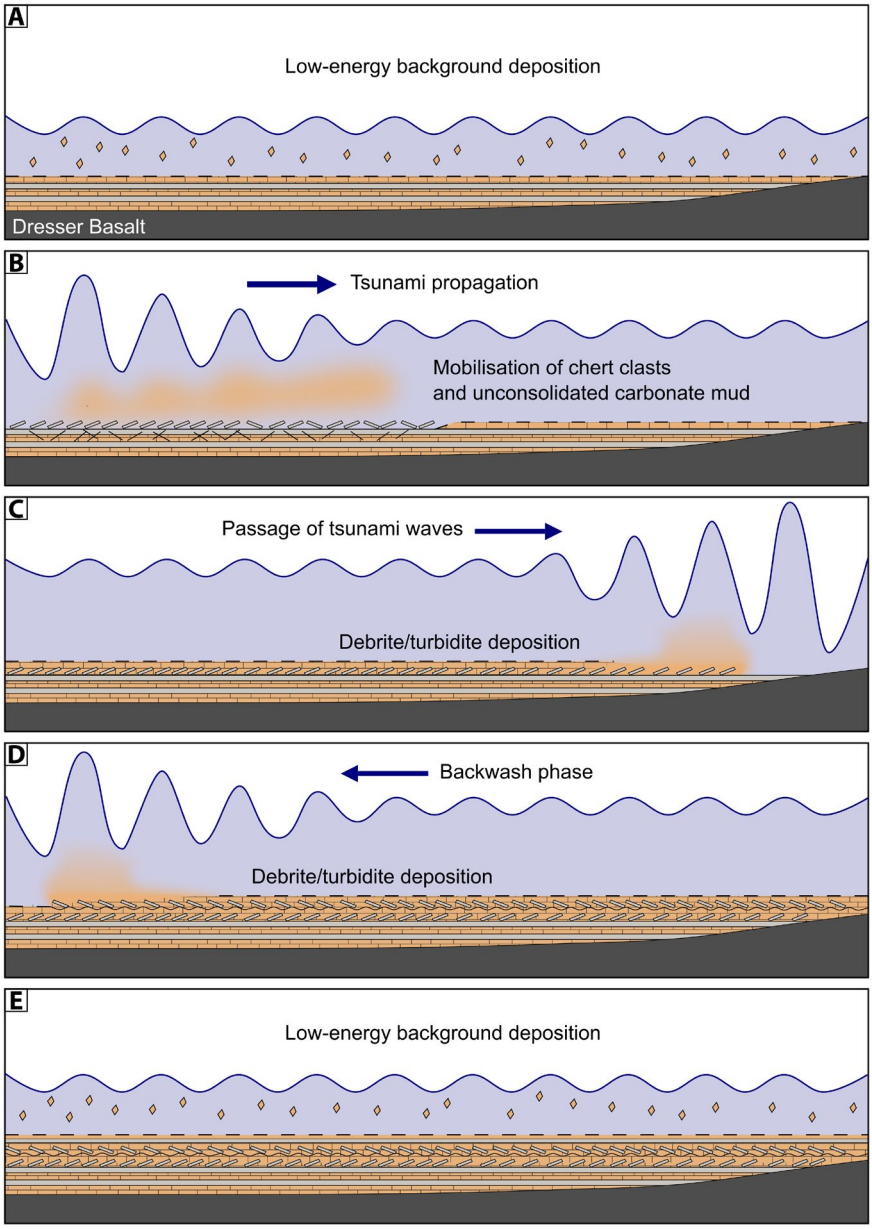

FIGURE 7 Sequence of depositional processes in the studied sedimentary section. (A) sedimentation of fine-grained carbonates and episodic silica under low-energy conditions forming; (B) initiation of a tsunami, mobilising carbonate mud and chert clasts from the sea floor; (C) deposition of the first debrite–turbidite couplet upon waning of current agitation; (D) deposition of the second debrite–turbidite couplet with reduced thickness due to energy loss upon wave rebound and partial erosion of lower subunit of Unit 2; (E) return to sedimentation of fine-grained carbonates under low-energy conditions. Carbonate deposits are marked by a brown brick signature, chert is marked in plain grey, and settling fine-grained carbonates are marked by brown rhombs. Unconsolidated deposits are marked by dashed lines

4.2 | Trigger mechanism

Tsunamis are triggered by geological events that cause either top-down (meteorite impacts, mass movements) or bottom-up (subaquatic earthquakes and volcanism) vertical displacement of the water column (Dawson & Stewart, 2007). The common association of previously reported Palaeoarchaean tsunami deposits with impact spherules or cosmochemical impact signatures suggests that those tsunamis were caused by large meteorite impacts (Hassler et al., 2000; Lowe, 2013). In the Dresser Formation succession studied here, no such evidence of an impact signature was observed. However, it is known that impact spherules are relatively unstable and often not preserved (Simonson & Glass, 2004); moreover, smaller impactors (<10 km in diameter) are not sufficient to produce a global spherule layer (Johnson & Melosh, 2012), while they may still trigger tsunami waves (Wünnemann et al., 2010). Geological archives may therefore not necessarily record impacts of extraterrestrial bodies, especially as many impactors in the early Archaean would have been smaller than those larger ones that left diagnostic fingerprints (see Lowe & Byerly, 2018). Hence, it is possible that the Dresser tsunami was triggered by an impact event, even though it did not leave a distinctive impact-related signature.

Alternatively, the most common triggers of tsunamis in the modern day by far are subduction zone earthquakes, since these often cause a rapid and significant vertical displacement of the water column (Dawson & Stewart, 2007; Elbanna et al., 2021). However, modern style subduction appears probably not to have been operative in the formation of the Palaeoarchaean Pilbara Craton, which has been documented to have formed as a volcanic plateau over a mantle plume (Van Kranendonk et al., 2002, 2019b). Thus, a subduction zone-generated earthquake appears an improbable trigger to have caused the Dresser Formation tsunami deposit.

Rather, a probable trigger of the Dresser Formation tsunami deposit is related to endogenic processes via local volcanic and/or seismic activity. Indeed, the Dresser Formation was deposited within a volcanically and tectonically active caldera basin affected by various types of volcanic activity (pillow basalts, volcanic ash layers, hydrothermal chert-barite-veins) and extensional deformation (syndepositional growth faults) during deposition (Nijman et al., 1999; Tadbiri & Van Kranendonk, 2020; Van Kranendonk et al., 2008, 2019a). The studied succession preserves no sedimentary or geochemical evidence for a volcanic eruption at the time of deposition, but more regional geological mapping indicates synsedimentary extensional growth faulting (Nijman et al., 1999; Tadbiri & Van Kranendonk, 2020; Van Kranendonk et al., 2019a, 2019b). It is therefore interpreted that seismic activity associated with extensional growth faulting may have triggered the tsunami event documented here, perhaps via secondary mass movements (Ward, 2001). This is consistent with deposition of the studied succession in a quiet-water interval, in between subaqueous lava eruption events (Figure 2). Moreover, the reworked sediments almost exclusively consist of chert and carbonates, equivalent to the unit directly underlying the tsunami deposit (Figures 2 through 5). This could indicate a nearby sediment source area and might support a rather local event. For these reasons, local seismic activity related to extensional growth faulting is regarded as the most plausible trigger of the Dresser tsunami event, although other generation mechanisms (i.e. meteorite impacts, volcanic eruptions) cannot be excluded.

4.3 | Possible influence of seawater chemistry on sedimentary processes

The presence of abundant chert beds in the studied succession (Figures 2 and 5) and elsewhere throughout the Palaeoarchaean successions of the Pilbara and Kaapvaal cratons (Ledevin, 2019; Van Kranendonk, 2006) indicates that Palaeoarchaean submarine sedimentation occurred under high SiO_2 (and bicarbonate) concentrations of seawater (Maliva et al., 2005; Siever, 1992). Highly SiO_2 enriched water is known from today's Lake Magadi in Kenya—a potential analogue for some Archaean hydrothermal environments (Reinhardt et al., 2019)—where evaporation of lake water causes the formation of brines with densities of up to 1.4 g/cm^3 (Eugster, 1970). In the Palaeoarchaean, active venting of silica-rich hydrothermal fluids was pervasive (Hofmann & Harris, 2008; Van Kranendonk, 2006), and perhaps particularly so in the restricted Dresser environment, resulting in even higher SiO_2 concentrations (cf. Tadbiri & Van Kranendonk, 2020; Van Kranendonk et al., 2008). As a consequence, the local seawater density was perhaps significantly higher than in Phanerozoic oceans. Regardless of the exact SiO_2 contents, it appears probable that a somewhat elevated density may have influenced hydrodynamic conditions in the Dresser Formation (e.g. current velocities, suspension of particles), including high-energy depositional processes. Nevertheless, a tsunami still seems like the most probable explanation for the observed sedimentological features.

4.4 | Implications for Early Earth

The studied section dates back to *ca* 3.48 Ga (Van Kranendonk et al., 2008) and thus predates the *ca* 3.47 Ga tsunami-reworked impact ejecta beds in the Onverwacht Group (Barberton Greenstone Belt: Byerly, 2002) and Warrawoona Group (Pilbara Craton: Glikson et al., 2004). Therefore, the studied example here represents the oldest

recorded tsunami deposit on Earth to date and further establishes the significance of high-energy depositional events for early Earth's habitats. If the tsunami event was triggered by the impact of an extraterrestrial body, then the deposit would also be the earliest geological evidence for an impact event. Regardless of the trigger mechanism, results presented here clearly corroborate the long-standing hypothesis that Earth's earliest surface environments were substantially affected by high-energy depositional events. Such events were important in shaping the habitats in which life emerged, for instance through the disturbance of surface sediments, or the redistribution of nutrients in the water column (Kanaya et al., 2015; Lowe et al., 2003; Noda et al., 2007). This study is thus an important contribution to understanding the emergence and survival of life on Earth and, perhaps, beyond.

5 | CONCLUSIONS

The *ca* 3.48 Ga old Dresser Formation (Pilbara Craton, Western Australia) provides a unique and valuable glimpse into Earth's earliest habitats. A previously undocumented, thin sedimentary succession within this formation that was deposited in a relatively deep-water setting below storm-wave base has been described. Particularly noteworthy in this succession is the presence of two clast-bearing debrite–turbidite couplets that exhibit bi-directional flow structures. These sedimentological features are best explained by high-energy inflow and backwash currents associated with a single tsunami event. The succession thus contains the oldest recorded tsunami deposit on Earth. Although no direct evidence for the trigger mechanism of this tsunami was found, the geological context suggests a possible role of seismic activity related to local extensional faulting. Collectively, these results testify that Earth's earliest habitats were affected by high-energy events such as tsunamis, and lend further support to the idea that such events were important in shaping the environments in which Earth's biosphere emerged.

ACKNOWLEDGEMENTS

This work was funded by the German Research Foundation (DFG) (grants Re 665/42-2, Th 713/13-2, Du 1450/3-1, Du 1450/3-2, 1450/7-1; all priority program (SPP)1833 'Building a habitable Earth'). MJVK was supported by The Australian Research Council (ARC) Centre of Excellence for Core to Crust Fluid Systems (CE1101017) and by ARC Discovery Project DP180103204. We thank Helge Mißbach for his participation in fieldwork, Nadine Schäfer for performing Raman spectroscopy and Axel Hackmann for preparing the thin sections. This is publication no. 13 of the Early Life Working Group (Department of Geobiology, University of Göttingen; Göttingen Academy of Sciences and Humanities). We thank P.J.M. Costa and an anonymous reviewer for their constructive comments which greatly improved this manuscript.

DATA AVAILABILITY STATEMENT

The data that support the findings of this study are available from the corresponding author upon request.

ORCID

Eric A. Runge https://orcid.org/0000-0003-1921-8678

REFERENCES

Arndt, N.T. & Nisbet, E.G. (2012) Processes on the young earth and the habitats of early life. *Annual Review of Earth and Planetary Sciences*, *40*, 521–549. https://doi.org/10.1146/annurev-earth-042711-105316

Bahlburg, H. & Spiske, M. (2012) Sedimentology of tsunami inflow and backflow deposits: key differences revealed in a modern example: tsunami deposits at Isla Mocha. *Sedimentology*, *59*, 1063–1086. https://doi.org/10.1111/j.1365-3091.2011.01295.x

Baumgartner, R.J., Van Kranendonk, M.J., Wacey, D., Fiorentini, M.L., Saunders, M., Caruso, S., Pages, A., Homann, M. & Guagliardo, P. (2019) Nano–porous pyrite and organic matter in 3.5-billion-year-old stromatolites record primordial life. *Geology*, *47*, 1039–1043. https://doi.org/10.1130/G46365.1

Benton, M.J. & Gray, D.I. (1981) Lower Silurian distal shelf storm-induced turbidites in the Welsh Borders: sediments, tool marks and trace fossils. *Journal of the Geological Society*, *138*, 675–694. https://doi.org/10.1144/gsjgs.138.6.0675

Bouma, A.H. (1962) *Sedimentology of some Flysch Deposits*. Amsterdam: Elsevier. 168 pp.

Byerly, G.R., Lowe, D.R., Wooden, J.L. & Xie, X. (2002) An Archean impact layer from the Pilbara and Kaapvaal Cratons. *Science*, *297*, 1325–1327. https://doi.org/10.1126/science.1073934

Costa, P.J.M. & Andrade, C. (2020) Tsunami deposits: present knowledge and future challenges. *Sedimentology*, *67*, 1189–1206. https://doi.org/10.1111/sed.12724

Costa, P., Andrade, C., Freitas, M., Oliveira, M., Lopes, V., Dawson, A., Moreno, J., Fatela, F. & Jouanneau, J.-M. (2012) A tsunami record in the sedimentary archive of the central Algarve coast, Portugal: characterizing sediment, reconstructing sources and inundation paths. *The Holocene*, *22*, 899–914. https://doi.org/10.1177/0959683611434227

Dawson, A.G. & Stewart, I. (2007) Tsunami deposits in the geological record. *Sedimentary Geology*, *200*, 166–183. https://doi.org/10.1016/j.sedgeo.2007.01.002

Djokic, T., Van Kranendonk, M.J., Campbell, K.A., Walter, M.R. & Ward, C.R. (2017) Earliest signs of life on land preserved in ca. 3.5 Ga hot spring deposits. *Nature Communications*, *8*, 15263. https://doi.org/10.1038/ncomms15263

Duda, J.-P., Thiel, V., Bauersachs, T., Mißbach, H., Reinhardt, M., Schäfer, N., Van Kranendonk, M.J. & Reitner, J. (2018) Ideas and perspectives: hydrothermally driven redistribution and sequestration of early Archaean biomass – the "hydrothermal pump hypothesis". *Biogeosciences*, *15*, 1535–1548. https://doi.org/10.5194/bg-15-1535-2018

Dumas, S. & Arnott, R.W.C. (2006) Origin of hummocky and swaley cross-stratification—the controlling influence of unidirectional current strength and aggradation rate. *Geology*, *34*, 1073. https://doi.org/10.1130/G22930A.1

Einsele, G., Chough, S.K. & Shiki, T. (1996) Depositional events and their records—an introduction. *Sedimentary Geology*, *104*, 1–9. https://doi.org/10.1016/0037-0738(95)00117-4

Elbanna, A., Abdelmeguid, M., Ma, X., Amlani, F., Bhat, H.S., Synolakis, C. & Rosakis, A.J. (2021) Anatomy of strike-slip fault tsunami genesis. *Proceedings of the National Academy of Sciences*, *118*, e2025632118. https://doi.org/10.1073/pnas.2025632118

Eugster, H.P. (1970) Chemistry and origin of the Brines of Lake Magadi, Kenya. *Mineralogical Society of America Special Paper*, *3*, 213–235.

Fujiwara, O. & Kamataki, T. (2007) Identification of tsunami deposits considering the tsunami waveform: an example of subaqueous tsunami deposits in Holocene shallow bay on southern Boso Peninsula, Central Japan. *Sedimentary Geology*, *200*, 295–313. https://doi.org/10.1016/j.sedgeo.2007.01.009

Glikson, A.Y., Allen, C. & Vickers, J. (2004) Multiple 3.47-Ga-old asteroid impact fallout units, Pilbara Craton, Western Australia. *Earth and Planetary Science Letters*, *221*, 383–396. https://doi.org/10.1016/S0012-821X(04)00104-9

Glikson, A., Hickman, A., Evans, N.J., Kirkland, C.L., Park, J.-W., Rapp, R. & Romano, S. (2016) A new ~3.46 Ga asteroid impact ejecta unit at Marble Bar, Pilbara Craton, Western Australia: a petrological, microprobe and laser ablation ICPMS study. *Precambrian Research*, *279*, 103–122. https://doi.org/10.1016/j.precamres.2016.04.003

Hassler, S.W., Robey, H.F. & Simonson, B.M. (2000) Bedforms produced by impact-generated tsunami, 2.6 Ga Hamersley basin, Western Australia. *Sedimentary Geology*, *135*, 283–294.

Hassler, S.W. & Simonson, B.M. (2001) The sedimentary record of extraterrestrial impacts in deep-shelf environments: evidence from the Early Precambrian. *The Journal of Geology*, *109*, 1–19. https://doi.org/10.1086/317958

Hofmann, A. & Harris, C. (2008) Silica alteration zones in the Barberton greenstone belt: a window into subseafloor processes 3.5–3.3 Ga ago. *Chemical Geology*, *257*, 221–239. https://doi.org/10.1016/j.chemgeo.2008.09.015

Ikehara, K., Irino, T., Usami, K., Jenkins, R., Omura, A. & Ashi, J. (2014) Possible submarine tsunami deposits on the outer shelf of Sendai Bay, Japan resulting from the 2011 earthquake and tsunami off the Pacific coast of Tohoku. *Marine Geology*, *358*, 120–127. https://doi.org/10.1016/j.margeo.2014.11.004

Jaffe, B.E., Goto, K., Sugawara, D., Richmond, B.M., Fujino, S. & Nishimura, Y. (2012) Flow speed estimated by inverse modeling of sandy tsunami deposits: results from the 11 March 2011 tsunami on the coastal plain near the Sendai Airport, Honshu, Japan. *Sedimentary Geology*, *282*, 90–109. https://doi.org/10.1016/j.sedgeo.2012.09.002

Johnson, B.C. & Melosh, H.J. (2012) Impact spherules as a record of an ancient heavy bombardment of Earth. *Nature*, *485*, 75–77. https://doi.org/10.1038/nature10982

Kanaya, G., Suzuki, T. & Kikuchi, E. (2015) Impacts of the 2011 Tsunami on sediment characteristics and Macrozoobenthic assemblages in a shallow eutrophic lagoon, Sendai Bay, Japan. *PLoS One*, *10*, e0135125. https://doi.org/10.1371/journal.pone.0135125

Kranendonk, M.J.V., Hickman, A.H., Smithies, R.H., Nelson, D.R. & Pike, G. (2002) Geology and tectonic evolution of the Archean North Pilbara Terrain, Pilbara Craton, Western Australia. *Economic Geology*, *97*, 695–732.

Krull Davatzes, A., Goderis, S. & Simonson, B.M. (2019) Archean asteroid impacts on earth. In Van Kranendonk, M.J., Bennett, V.C. & Hoffmann, J.E. (Eds.) *Earth's oldest rocks*. Amsterdam: Elsevier, pp. 169–185. doi:https://doi.org/10.1016/B978-0-444-63901-1.00008-3

Ledevin, M. (2019) Archean cherts. In: Van Kranendonk, M.J., Bennett, V.C. & Hoffmann, J.E. (Eds.), *Earth's oldest rocks*. Amsterdam: Elsevier, pp. 913–944. doi:https://doi.org/10.1016/B978-0-444-63901-1.00037-X

Lepot, K. (2020) Signatures of early microbial life from the Archean (4 to 2.5 Ga) eon. *Earth-Science Reviews*, *209*, 103296. https://doi.org/10.1016/j.earscirev.2020.103296

Lowe, D.R. (1980) Stromatolites 3,400-Myr old from the Archean of Western Australia. *Nature*, *284*, 441–443. https://doi.org/10.1038/284441a0

Lowe, D.R. (1982) Sediment gravity flows: ii depositional models with special reference to the deposits of high-density turbidity currents. *SEPM Journal of Sedimentary Research*, *52*. doi:https://doi.org/10.1306/212F7F31-2B24-11D7-8648000102C1865D

Lowe, D.R. (2013) Crustal fracturing and chert dike formation triggered by large meteorite impacts, ca. 3.260 Ga, Barberton Greenstone Belt, South Africa. *Geological Society of America Bulletin*, *125*, 894–912. https://doi.org/10.1130/B30782.1

Lowe, D.R. & Byerly, G.R. (2018) The terrestrial record of Late Heavy Bombardment. *New Astronomy Reviews*, *81*, 39–61. https://doi.org/10.1016/j.newar.2018.03.002

Lowe, D.R., Byerly, G.R., Kyte, F.T., Shukolyukov, A., Asaro, F. & Krull, A. (2003) Spherule beds 3.47–3.24 billion years old in the Barberton Greenstone Belt, South Africa: a record of large meteorite impacts and their influence on early crustal and biological evolution. *Astrobiology*, *3*, 7–48. https://doi.org/10.1089/153110703321632408

Maliva, R.G., Knoll, A.H. & Simonson, B.M. (2005) Secular change in the Precambrian silica cycle: insights from chert petrology. *Geological Society of America Bulletin*, *117*, 835–845. https://doi.org/10.1130/B25555.1

Mata, S.A. & Bottjer, D.J. (2012) Facies control on lower Cambrian wrinkle structure development and paleoenvironmental distribution, southern Great Basin, United States. *Facies*, *59*, 631–651. https://doi.org/10.1007/s10347-012-0331-3

Mißbach, H., Duda, J.-P., van den Kerkhof, A.M., Lüders, V., Pack, A., Reitner, J. & Thiel, V. (2021) Ingredients for microbial life preserved in 3.5 billion-year-old fluid inclusions. *Nature Communications*, *12*, 1101. https://doi.org/10.1038/s41467-021-21323-z

Morton, R.A., Gelfenbaum, G. & Jaffe, B.E. (2007) Physical criteria for distinguishing sandy tsunami and storm deposits using modern examples. *Sedimentary Geology*, *200*, 184–207. https://doi.org/10.1016/j.sedgeo.2007.01.003

Nijman, W., de Bruijne, H. & Valkering, M.E. (1999) Growth fault control of Early Archaean cherts, barite mounds and chert-barite veins, North Pole Dome, Eastern Pilbara, Western Australia. *Precambrian Research*, *95*, 247–274.

Noda, A., Katayama, H., Sagayama, T., Suga, K., Uchida, Y., Satake, K., Abe, K. & Okamura, Y. (2007) Evaluation of tsunami impacts on shallow marine sediments: An example from the tsunami caused by the 2003 Tokachi-oki earthquake, northern Japan.

Sedimentary Geology, *200*, 314–327. https://doi.org/10.1016/j.sedgeo.2007.01.010

Reinhardt, M., Goetz, W., Duda, J.-P., Heim, C., Reitner, J. & Thiel, V. (2019) Organic signatures in Pleistocene cherts from Lake Magadi (Kenya), analogs for early Earth hydrothermal deposits. *Biogeosciences*, *16*, 2443–2465. doi:https://doi.org/10.5194/bg-2018-513

Riou, B., Chaumillon, E., Chagué, C., Sabatier, P., Schneider, J.-L., Walsh, J.-P., Zawadzki, A. & Fierro, D. (2020) Backwash sediment record of the 2009 South Pacific Tsunami and 1960 Great Chilean Earthquake Tsunami. *Scientific Reports*, *10*, 4149. https://doi.org/10.1038/s41598-020-60746-4

Riou, B., Chaumillon, E., Schneider, J., Corrège, T. & Chagué, C. (2018) The sediment-fill of Pago Pago Bay (Tutuila Island, American Samoa): new insights on the sediment record of past tsunamis. *Sedimentology*, *67*, 1577–1600. https://doi.org/10.1111/sed.12574

Siever, R. (1992) The silica cycle in the Precambrian. *Geochimica et Cosmochimica Acta*, *56*, 3265–3272. https://doi.org/10.1016/0016-7037(92)90303-Z

Simonson, B.M. & Glass, B.P. (2004) Spherule layers – records of ancient impacts. *Annual Review of Earth and Planetary Sciences*, *32*, 329–361. https://doi.org/10.1146/annurev.earth.32.101802.120458

Tada, R., Nakano, Y., Iturralde-Vinent, M.A., Yamamoto, S., Kamata, T., Tajika, E., Toyoda, K. et al. (2002) Complex tsunami waves suggested by the Cretaceous-Tertiary boundary deposit at the Moncada section, western Cuba. In: Koeberl, C. & MacLeod, K.G. (Eds.) *Catastrophic events and mass extinctions: impacts and beyond*. Geological Society of America Special Paper, vol. *356*. Boulder: Geological Society of America, pp. 109–123. https://doi.org/10.1130/0-8137-2356-6.109

Tadbiri, S. & Van Kranendonk, M.J. (2020) Structural analysis of syn-depositional hydrothermal veins of the 3.48 Ga Dresser Formation, Pilbara Craton, Australia. *Precambrian Research*, *347*, 105844. https://doi.org/10.1016/j.precamres.2020.105844

Ueno, Y., Ono, S., Rumble, D. & Maruyama, S. (2008) Quadruple sulfur isotope analysis of ca. 3.5Ga Dresser Formation: new evidence for microbial sulfate reduction in the early Archean. *Geochimica et Cosmochimica Acta*, *72*, 5675–5691. https://doi.org/10.1016/j.gca.2008.08.026

Van Kranendonk, M.J. (2006) Volcanic degassing, hydrothermal circulation and the flourishing of early life on Earth: a review of the evidence from c. 3490–3240 Ma rocks of the Pilbara Supergroup, Pilbara Craton, Western Australia. *Earth-Science Reviews*, *74*, 197–240. https://doi.org/10.1016/j.earscirev.2005.09.005

Van Kranendonk, M., Philippot, P., Lepot, K., Bodorkos, S. & Pirajno, F. (2008) Geological setting of Earth's oldest fossils in the ca. 3.5 Ga Dresser Formation, Pilbara Craton, Western Australia. *Precambrian Research*, *167*, 93–124. https://doi.org/10.1016/j.precamres.2008.07.003

Van Kranendonk, M.J., Smithies, R.H. & Champion, D.C. (2019b) Paleoarchean development of a continental nucleus: the East Pilbara Terrane of the Pilbara Craton, Western Australia. In: Van Kranendonk, M.J., Bennett, V.C. & Hoffmann, J.E. (Eds.) *Earth's Oldest Rocks*. Amsterdam: Elsevier, pp. 437–462.

Van Kranendonk, M.J., Djokic, T., Poole, G., Tadbiri, S., Steller, L. & Baumgartner, R. (2019a) Depositional Setting of the Fossiliferous, c.3480 Ma Dresser Formation, Pilbara Craton. In Van Kranendonk, M.J., Bennett, V.C. & Hoffmann, J.E. (Eds.) *Earth's oldest rocks*. Elsevier, pp. 985–1006. doi:https://doi.org/10.1016/B978-0-444-63901-1.00040-X

Walker, R.G. (1978) Deep-water sandstone facies and ancient submarine fans: models for exploration for stratigraphic traps. *AAPG Bulletin*, *62*. doi:https://doi.org/10.1306/C1EA4F77-16C9-11D7-8645000102C1865D

Ward, S.N. (2001) Landslide tsunami. *Journal of Geophysical Research: Solid Earth*, *106*, 11201–11215. https://doi.org/10.1029/2000JB900450

Weiss, R. & Bahlburg, H. (2006) A note on the preservation of offshore tsunami deposits. *Journal of Sedimentary Research*, *76*, 1267–1273. https://doi.org/10.2110/jsr.2006.110

Wünnemann, K., Collins, G.S. & Weiss, R. (2010) Impact of a cosmic body into earth's ocean and the generation of large tsunami waves: insight from numerical modeling. *Reviews of Geophysics*, *48*, RG4006. https://doi.org/10.1029/2009RG000308

How to cite this article: Runge, E.A., Duda, J.-P., Van Kranendonk, M.J. & Reitner, J. (2022) Earth's oldest tsunami deposit? Early Archaean high-energy sediments in the *ca* 3.48 Ga Dresser Formation (Pilbara, Western Australia). *The Depositional Record*, 00, 1–13. https://doi.org/10.1002/dep2.175